Perovskite Nanostructures

International Edition: DOI: 10.1002/anie.201605909
German Edition: DOI: 10.1002/ange.201605909

Highly Luminescent Cesium Lead Halide Perovskite Nanocrystals with Tunable Composition and Thickness by Ultrasonication

Yu Tong, Eva Bladt, Meltem F. Aygüler, Aurora Manzi, Karolina Z. Milowska, Verena A. Hintermayr, Pablo Docampo, Sara Bals, Alexander S. Urban,* Lakshminarayana Polavarapu,* and Jochen Feldmann*

Abstract: *We describe the simple, scalable, single-step, and polar-solvent-free synthesis of high-quality colloidal $CsPbX_3$ (X = Cl, Br, and I) perovskite nanocrystals (NCs) with tunable halide ion composition and thickness by direct ultrasonication of the corresponding precursor solutions in the presence of organic capping molecules. High angle annular dark field scanning transmission electron microscopy (HAADF-STEM) revealed the cubic crystal structure and surface termination of the NCs with atomic resolution. The NCs exhibit high photoluminescence quantum yields, narrow emission line widths, and considerable air stability. Furthermore, we investigated the quantum size effects in $CsPbBr_3$ and $CsPbI_3$ nanoplatelets by tuning their thickness down to only three to six monolayers. The high quality of the prepared NCs ($CsPbBr_3$) was confirmed by amplified spontaneous emission with low thresholds. The versatility of this synthesis approach was demonstrated by synthesizing different perovskite NCs.*

The outstanding optoelectronic properties of inexpensive and solution-processable hybrid metal halide perovskites have brought them to the forefront of many research fields, such as solar cells, light-emitting diodes, photodetectors, and lasers.[1] One of the main advantages of these materials is the fact that the optical band gap can be easily tuned by exchanging individual components.[2] The success of these materials quickly led to the synthesis of nanocrystals (NCs), first in the form of organic/inorganic hybrid perovskites,[1b,3] and later also as purely inorganic cesium-based perovskites.[4] Nanocrystals exhibit high photoluminescence quantum yields (PLQYs) and offer an inherent way to tune the optical properties through size- and dimensionality-dependent quantum confinement.[5] Currently, unlike for conventional metal chalcogenide based NCs, only a limited number of synthetic methods are available for the preparation of $CsPbX_3$ NCs. The most widely adopted method for the preparation of $CsPbX_3$ nanocubes with very high PLQYs is based on high-temperature hot injection, which was developed by Kovalenko and co-workers in 2015 and refined by Alivisatos and co-workers to obtain nanoplatelets (NPLs).[4b,6] However, the hot-injection approach is tedious, it is generally performed under an inert atmosphere, and can currently only be applied to control the thickness of bromine-based perovskites. Indeed, an additional halide ion exchange step is necessary to prepare NPLs based on iodide or chloride perovskites, as shown simultaneously by the groups of Manna, Kovalenko, and Alivisatos.[4b,6,7] Sun et al.[8] reported an approach for the shape-controlled synthesis of $CsPbBr_3$ NCs at room temperature. However, this method requires the pre-synthesis of the cesium precursor under inert atmosphere at higher temperatures. While being simple, room-temperature syntheses generally lead to NCs with relatively low PLQYs.[8] Herein, we describe a versatile, polar-solvent-free, single-step approach for the large-scale synthesis of highly luminescent $CsPbX_3$ perovskite NCs and NPLs. Both the halide composition and the NPL thickness can be tuned, namely by direct ultrasonication of the corresponding precursors in the presence of organic ligands (Figure 1 a). The ability to tune the thickness revealed the quantum size effects operating in $CsPbX_3$ (X = Br and I) NPLs, which enabled us to investigate the thickness dependence of the optical properties of $CsPbI_3$ NPLs for the first time.

As shown in Figure 1 a, our synthesis of $CsPbX_3$ (X = Cl, Br, and I) perovskite NCs is based on direct tip sonication of mixtures of the corresponding precursor salts (Cs_2CO_3 and PbX_2) and capping ligands (oleylamine and oleic acid) in a nonpolar solvent (mineral oil or octadecene) under ambient atmospheric conditions. Such a sonication process has previously been used for the preparation of metal nanoparticles. This method is based on metal–ligand complex formation under ultrasonication; these complexes are then further

[*] Y. Tong, A. Manzi, V. A. Hintermayr, Dr. A. S. Urban, Dr. L. Polavarapu, Prof. Dr. J. Feldmann
Chair for Photonics and Optoelectronics
Department of Physics and Center for NanoScience (CeNS)
Ludwig-Maximilians-Universität
Amalienstrasse 54, 80799 Munich (Germany)
E-mail: urban@lmu.de
l.polavarapu@lmu.de
Y. Tong, A. Manzi, Dr. A. S. Urban, Dr. L. Polavarapu, Prof. Dr. J. Feldmann
Nanosystems Initiative Munich (NIM)
Schellingstrasse 4, 80799 Munich (Germany)
E. Bladt, Prof. Dr. S. Bals
EMAT, University of Antwerp
Groenenborgerlaan 171, B-2020 Antwerp (Belgium)
E-mail: sara.bals@uantwerpen.be
M. F. Aygüler, Prof. Dr. P. Docampo
Department of Chemistry and Center for NanoScience (CeNS)
Ludwig-Maximilians-Universität (LMU)
Butenandtstrasse 5–13, 81377 Munich (Germany)
Dr. K. Z. Milowska
Department of Materials Science and Metallurgy
University of Cambridge
27 Charles Babbage Rd, Cambridge CB3 0FS (UK)
Supporting information and the ORCID identification number(s) for the author(s) of this article can be found under: http://dx.doi.org/10.1002/anie.201605909.

 © 2016 Wiley-VCH Verlag GmbH & Co. KGaA, Weinheim

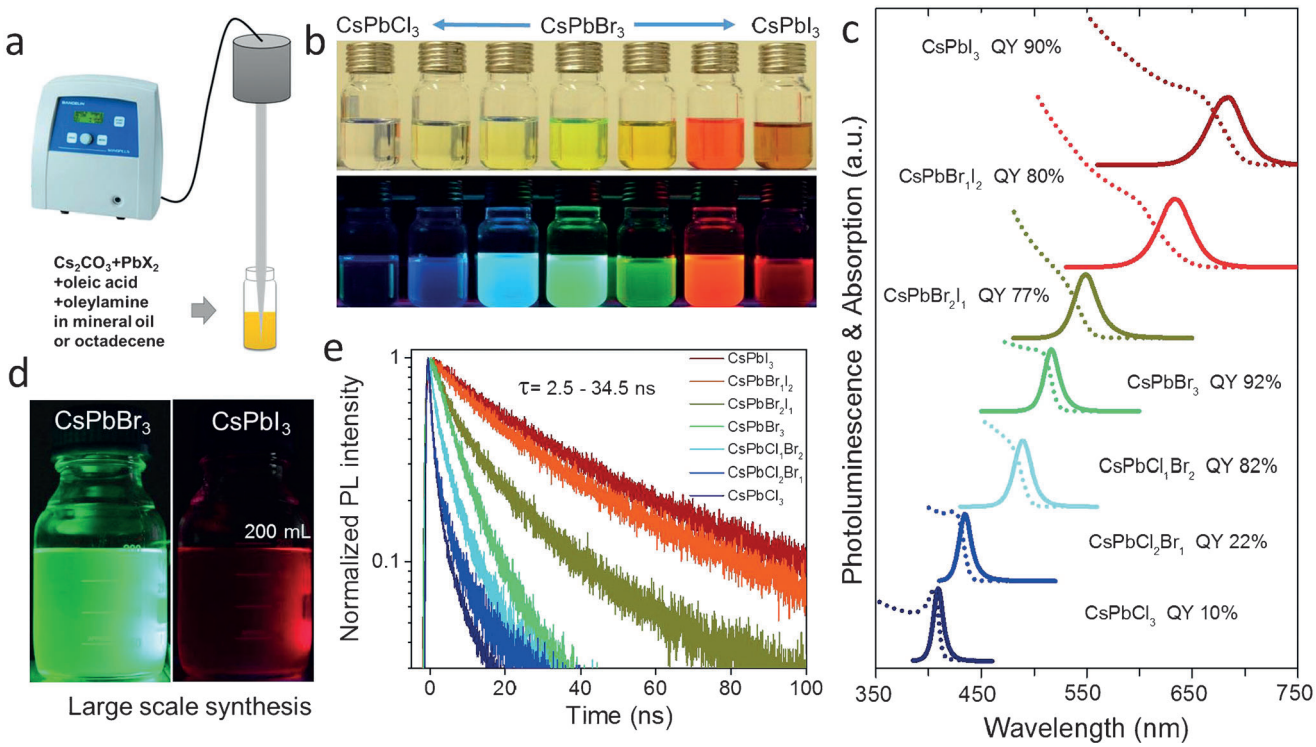

Figure 1. a) Synthesis of $CsPbX_3$ NCs through single-step tip sonication. b) Photograph of colloidal dispersions of $CsPbX_3$ NCs with different halide (X = Cl, Br, and I) compositions in hexane under room light (top) and UV light (bottom, $\lambda = 367$ nm). c) Corresponding UV/Vis and PL spectra and PLQYs of the samples shown in (b). d) Scalable synthesis of NCs (by a factor of up to 10). Photograph of $CsPbBr_3$ and $CsPbI_3$ colloidal dispersions under UV light. e) PL decay dynamics of the NCs shown in (b). Calculated $\tau \approx 2.5$–34.5 ns.

reduced into metal nanoparticles. In the present system, sonication induces the formation of a cesium–oleate complex that is soluble in nonpolar solvents and reacts with PbX_2 in the presence of oleylamine and oleic acid to yield colloidal $CsPbX_3$ NCs in a one-pot-process directly from their precursors (see the Supporting Information, Figure S1). Purified colloidal dispersions of $CsPbX_3$ (X = Cl, Br, I, Cl/Br, and Br/I) perovskite NCs in hexane under room light as well as UV light are shown in Figure 1b. The PL emission color varies from blue to green to red as the halide composition of the precursors changes from Cl to Br to I (Figures 1b and S1). The synthesis can be easily scaled up by scaling up each of the reaction components by tenfold. The optical properties of the colloidal dispersions obtained in this manner hardly differed from those obtained under the original conditions (Figures 1c and S2).

The color changes observed upon varying the halide content were quantified by UV/Vis absorption and fluorescence spectroscopy (Figure 1c). The prepared dispersions exhibited narrow, single-peak PL emission with a full width at half maximum (FWHM) of 12–40 nm. The UV/Vis spectra showed a single, steep absorption onset, which was only slightly red-shifted from the PL maximum. These observations clearly show that the dispersions only contain NCs with single halide composition and not NCs with varying halide contents. Furthermore, the optical band gap energy can be tuned across almost the entire visible range (ca. 410–700 nm) by adjusting the halide composition. Moreover, the samples containing only Br or I exhibited high PLQYs of over 90%, whereas the mixed halides $CsPbBr_xCl_{3-x}$ ($x \geq 2$) had considerably lower PLQYs of only 10–25% (Figure 1c). Additionally, all colloidal dispersions except $CsPbI_3$ appeared to be stable for several months with a slight reduction in their PLQYs (Figure S3 and Table S1). $CsPbI_3$ NCs were gradually transformed into a non-fluorescent yellow phase after two months of storage under atmospheric conditions. It has previously been shown that mixed-halide organic/inorganic perovskite NCs exhibit phase separation under light illumination;[9] however, these inorganic perovskites seemed to be stable under continuous light irradiation (Figure S4). Time-resolved PL measurements of $CsPbX_3$ NCs revealed multi-exponential decay traces with average lifetimes in the range of 2.5–34.4 ns and with an inverse correlation between the halide-ion-controlled band gap and the decay lifetime. Combining the PL decay times and the PLQYs shows that whereas the iodide- and bromide-containing NCs are of high optical quality with nearly no non-radiative decay, the NCs with a high chloride content undergo significant non-radiative decay. The observed trends in the PLQYs and decay rates can be ascribed to the intrinsic optical properties of the halide perovskites.[2c]

Further proof for the high quality of the prepared NCs was obtained by electron microscopy. Bright field transmission electron microscopy (BF-TEM) overview images of $CsPbBr_3$ (Figure 2a) and $CsPbI_3$ (Figure 2d) NCs show well-defined cubic and rectangular shapes in projection (see Figure S5 for TEM images of mixed-halide perovskite NCs). The average crystal sizes are in the range of 10–

 © 2016 Wiley-VCH Verlag GmbH & Co. KGaA, Weinheim

These are not the final page numbers!

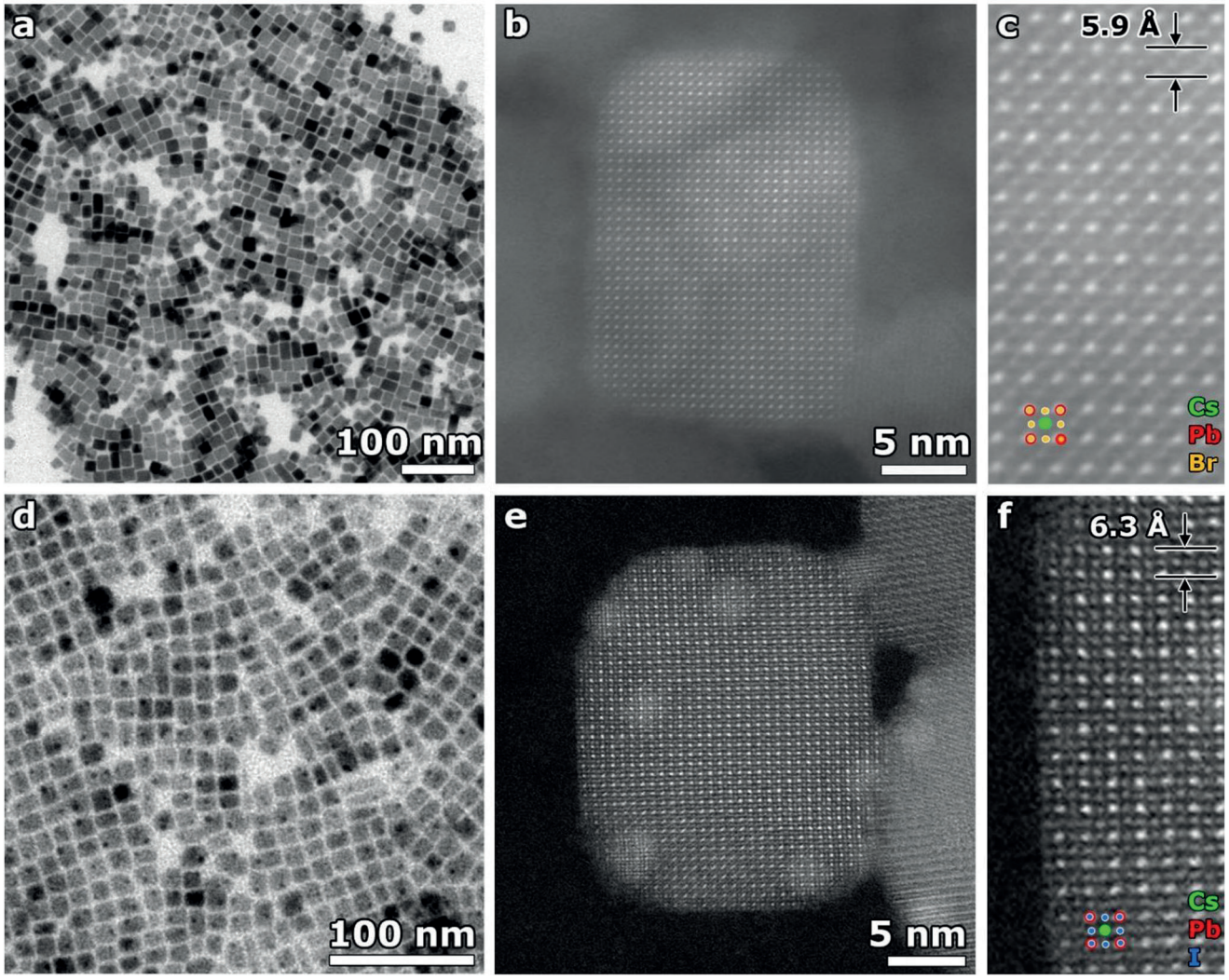

Figure 2. a, d) BF-TEM overview images of $CsPbBr_3$ and $CsPbI_3$ NCs, respectively. b, e) Atomically resolved high-resolution HAADF-STEM images of single $CsPbBr_3$ and $CsPbI_3$ NCs with more detailed views shown in (c) and (f), respectively.

15 nm and 8–12 nm for $CsPbBr_3$ and $CsPbI_3$, respectively. The prepared $CsPbBr_3$ NCs are rather monodisperse with an average size of 14.3 ± 1.3 nm, and are slightly larger than the NCs (ca. 11 nm) obtained by hot injection (Figure S6).[6] By terminating the synthesis at specific reaction times and by acquiring TEM images of the $CsPbBr_3$ NCs present in each solution, we found that the particle size gradually increased with reaction time, indicating seeded growth (Figure S7). The crystal structures of the different NCs were investigated by high angle annular dark field scanning transmission electron microscopy (HAADF-STEM) imaging. An atomic-resolution HAADF-STEM image of a $CsPbBr_3$ NC acquired along the [100] direction shows that the NC is single-crystalline and exhibits a cubic crystal structure with a lattice parameter of 5.9 Å (Figure 2b, c). The presence of Cs, Pb, and Br in the $CsPbBr_3$ NCs was confirmed by energy-dispersive X-ray spectroscopy (EDX) mapping (Figure S8). Like their bromide counterparts, the $CsPbI_3$ NCs were found to exhibit high crystallinity and a cubic crystal structure with a lattice spacing of 6.3 Å (Figure 2e, f). It is well known that $CsPbX_3$ NCs can crystallize in cubic, tetragonal, and orthorhombic polymorphs of the perovskite crystal lattice. After analyzing the crystal structures of a significant number of particles by using high-resolution HAADF-STEM, we found that all of the NCs are single crystals and mostly adopt the cubic perovskite phase regardless of the morphology (Figure S9) or composition (Figure S10). This result was further confirmed by XRD measurements performed on nanocrystalline thin films (Figure S11) and powders (Figure S12). Considering the detailed view of the HAADF-STEM image of the iodide NC in Figure 2 f, we suggest that the surface termination consists of Cs and I ions (Figure 2 f and Figure S13). This provides some indication with regard to the ligand binding mechanism, which has not been fully understood thus far. As the crystal is terminated with Cs atoms, it is most likely that the NCs are passivated by Cs-bound alkyl chains, for example, Cs oleate (Figure S13).

By varying the initial conditions of the synthesis, we were able to change the fluorescence of the dispersions from a dark red to a bright orange color for the $CsPbI_3$ NCs. Reducing the

 © 2016 Wiley-VCH Verlag GmbH & Co. KGaA, Weinheim

Cs_2CO_3/PbI_2 led to a blue shift of the emission of the resulting perovskite dispersions, with some of the dispersions displaying extremely broad PL spectra with multiple high-energy emission bands (Figure 3a). The new maxima are not shifted as the precursor ratio is changed; instead, their relative intensities change. In the extreme case, we are left with a single PL peak at 600 nm, constituting a nearly 100 nm shift from the original PL maximum at 685 nm. In UV/Vis measurements, a pronounced excitonic peak emerged, slightly red-shifted from the respective PL maximum. To investigate the origin of this PL, we recorded TEM images of the NCs in each sample (Figures 3b–e and S14). For the initial sample (1:3 precursor ratio), we observed cubic NCs with a size of 10–12 nm. As the Cs_2CO_3 content was reduced, very thin structures were observed along with the cubic NCs. The lower the Cs content is, the larger the amount of these nanostructures, which also become thinner and less polydisperse. In the extreme case, a nearly homogeneous distribution of nanocrystals with a size of 10×2 nm was observed, strongly reminiscent of perovskite NPLs.

Furthermore, as the precursor ratio was varied, additional scattering peaks emerged at low angles in the XRD measurements (Figure S14 and Tables S2–S4), a likely indication of 2D nanocrystal formation.[10] It has previously been demonstrated by two groups that $CsPbBr_3$ NPLs with controlled thickness can be prepared by performing the NC growth at low temperatures.[4b,7] In our method, it is most likely that the lower cesium content reduces the reaction rate and strongly favors 2D growth, producing NPLs. To the best of our knowledge, our work here constitutes the first report on the direct synthesis of highly fluorescent (ca. 75% PLQY) $CsPbI_3$ NPLs with controlled thickness, enabling studies of the thickness dependence of the excitonic properties of $CsPbI_3$ NPLs for the first time.

To validate the hypothesis that the NPLs are responsible for the blue-shifted PL, the positions of the individual PL maxima were plotted versus the projected thickness of the NPLs, and a theoretical study was conducted for comparison with the experimental data. The lowest experimentally observed PL band was ascribed to an NPL with a thickness of three layers ($n = 3$), as the approximate thickness of 2 nm from the TEM images is in excellent agreement with the thickness expected for three unit cells (ca. 1.89 nm). Higher-order peaks were then ascribed to incrementally thicker NPLs (Figures 3a and S15). HAADF-STEM imaging of an intermediate sample displaying multiple emission peaks confirmed the presence of cubic-phase single-crystalline nanoplatelets (Figures S16 and S17). The thickness of the platelets, which was found to vary from four to six unit cells, was determined from high-resolution HAADF-STEM images of standing

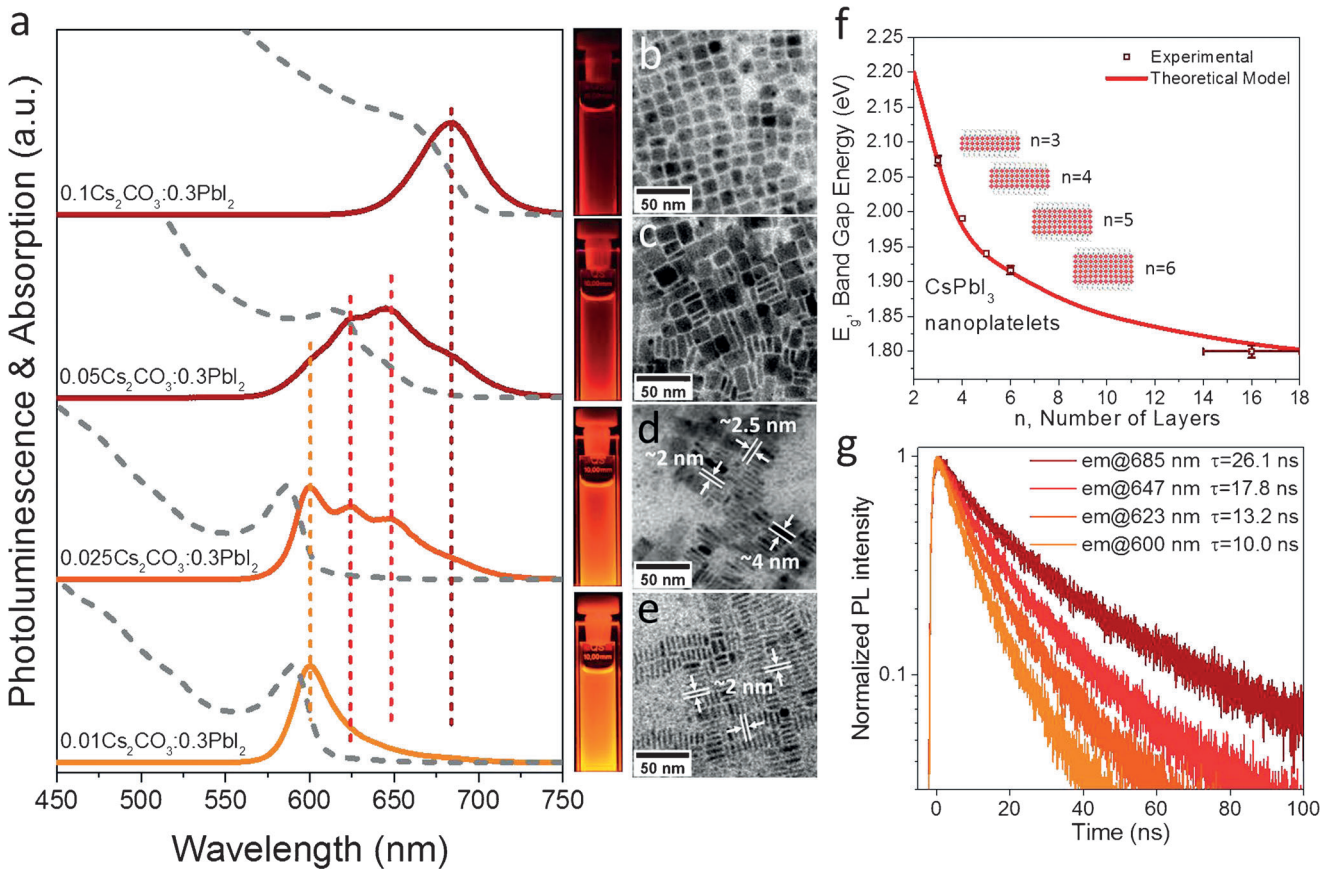

Figure 3. Tuning the optical properties by thickness control: UV/Vis absorption and PL spectra of $CsPbI_3$ NCs prepared from different Cs_2CO_3/PbI_2 ratios (a) and the corresponding TEM images (b–e). f) Calculated and experimental band gap energies of the perovskite NPLs as a function of the number of unit cells in the perovskite nanoplatelets. g) PL dynamics of a mixture of $CsPbI_3$ nanoplatelets with different thicknesses (prepared with 0.025 mmol of Cs_2CO_3 and 0.3 mmol PbI_2) probed at their emission maxima ($\lambda_{max} = 600$, 623, 647, and 685 nm.)

© 2016 Wiley-VCH Verlag GmbH & Co. KGaA, Weinheim

These are not the final page numbers!

platelets (Figure S17). It should be noted that the platelets are extremely sensitive to the electron beam, and that they tend to degrade and lose their crystallinity during acquisition (Figure S18). By high-resolution HAADF-STEM imaging, we are able to identify the emerging spherical nanoparticles as lead particles (Figure S19), as seen previously for organic–inorganic perovskites.[5a] For the bulk-like NCs, we estimated the mean thickness to be 16 layers, corresponding to roughly 10 nm large NCs. An established theoretical model was used to calculate the expected PL positions (see the Supporting Information for details).[5a] The experimental results and our calculations were in extremely good agreement (Figure 3 f), showing that the NCs observed in the dispersions are in fact responsible for the observed fluorescence. Time-resolved PL measurements were performed on the NPL colloidal dispersions, which were diluted enough to prevent both non-radiative energy transfer and reabsorption of PL in the dispersion. As shown for the case of a sample with many PL peaks (0.025 mmol Cs_2CO_3), we probed the PL decay of the PL maxima corresponding to NPLs of a particular thickness using time-correlated single photon counting (TCSPC) coupled with a monochromator. The traces had a multiexponential form with average lifetimes between 27 and 10 ns, which decreased with a decrease in the thickness of the nanoplatelets likely owing to an increase in the exciton binding energy in the strongly confined nanostructures (Figure 3 g). This behavior is similar to that discussed in epitaxial GaAs quantum wells.[11] Furthermore, this synthetic process is applicable to the preparation of $CsPbBr_3$ nanoplatelets (Figure S20). We obtained similar results with blue-shifted PL peaks for the highly emissive dispersions. We were again able to correlate this emission with theoretical values, corroborating the thickness dependence.

The high PLQYs and large absorption cross-sections of the NCs suggest that they should be promising materials for lasing applications with low thresholds for optical gain.[5h] To this end, we investigated the emergence of amplified spontaneous emission (ASE) in films containing $CsPbBr_3$ NCs (Figure 4). Upon excitation of the NCs at 400 nm with a femtosecond-pulsed laser, we observed the normal PL band at low fluences. At higher laser powers, a new, narrow band (FWHM: 3–7 nm) emerged on the low-energy side of the PL peak, red-shifted by about 15–20 nm owing to band gap renormalization and rapidly increasing in intensity as the pump power is increased (Figure 4 a). By plotting the integrated intensity of the fluorescence versus the pump fluence, we observed a clear threshold behavior with an onset for ASE at 2.1 $\mu J\,cm^{-2}$ (Figure 4 b). This is comparable to values reported for $CsPbX_3$ NCs prepared by using the hot-injection technique[5h] and lower than the values reported for surface-passivated $CsPbBr_3$ NCs.[12] Our studies clearly demonstrate that these NCs are excellent candidates for light-emitting applications. In an attempt to remove the lead, one of the remaining large challenges in the perovskite field,[13] we applied this synthesis for the preparation of $CsSnBr_3$ nanocrystals, which were highly monodisperse, but proved to be slightly unstable (Figure S21). Furthermore, the versatility of this synthesis approach was further demonstrated by the preparation of $CH_3NH_3PbBr_3$ NCs (Figure S22).

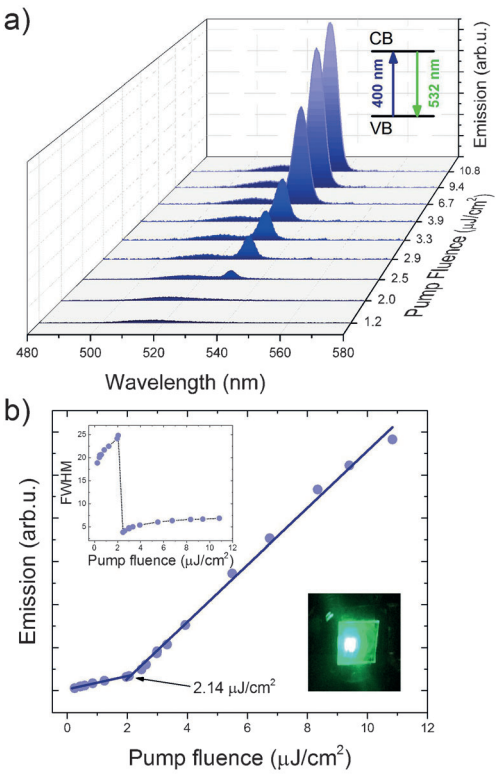

Figure 4. a) Pump-fluence-dependent PL emission (evolution of ASE) from a $CsPbBr_3$ NC film and b) the corresponding emission intensity at 530 nm. Inset: FWHM. All of the spectra were obtained with 400 nm femtosecond laser excitation.

In summary, we have presented a polar-solvent-free and scalable single-step solution-phase synthesis of highly luminescent $CsPbX_3$ perovskite NCs with photoluminescence tunable across the visible spectrum (400–700 nm). The cubic crystal structure and atomically precise surface termination of the NCs were revealed by high-resolution HAADF-STEM imaging. Furthermore, we have shown the quantum size effect operating in the $CsPbBr_3$ and $CsPbI_3$ nanoplatelets. The fact that these NCs exhibit a low-threshold ASE constitutes a further proof of their high quality. Importantly, we have further demonstrated that this simple synthesis approach can be extended by replacing all components of the perovskite in turn.

Acknowledgements

This work was supported by the Bavarian State Ministry of Science, Research, and Arts through the grant "Solar Technologies go Hybrid (SolTech)", the China Scholarship Council (Y.T.), the Alexander von Humboldt-Stiftung (L.P.), the European Union through the award of a Marie Curie Intra-European Fellowship (P.D.), the Scientific and Technological Research Council of Turkey (M.A.), the Flemish Fund for Scientific Research (FWO Vlaanderen; E.B.), and the European Research Council (S.B.; ERC Starting Grant 335078-COLOURATOMS).

 © 2016 Wiley-VCH Verlag GmbH & Co. KGaA, Weinheim

Keywords: HAADF-STEM · nanocrystals · perovskites · quantum confinement · ultrasonication

[1] a) M. M. Lee, J. Teuscher, T. Miyasaka, T. N. Murakami, H. J. Snaith, *Science* **2012**, *338*, 643 – 647; b) L. C. Schmidt, A. Pertegas, S. Gonzalez-Carrero, O. Malinkiewicz, S. Agouram, G. M. Espallargas, H. J. Bolink, R. E. Galian, J. Perez-Prieto, *J. Am. Chem. Soc.* **2014**, *136*, 850 – 853.

[2] a) V. D'Innocenzo, A. R. Srimath Kandada, M. De Bastiani, M. Gandini, A. Petrozza, *J. Am. Chem. Soc.* **2014**, *136*, 17730 – 17733; b) G. E. Eperon, S. D. Stranks, C. Menelaou, M. B. Johnston, L. M. Herz, H. J. Snaith, *Energy Environ. Sci.* **2014**, *7*, 982 – 988; c) Q. A. Akkerman, V. D'Innocenzo, S. Accornero, A. Scarpellini, A. Petrozza, M. Prato, L. Manna, *J. Am. Chem. Soc.* **2015**, *137*, 10276 – 10281.

[3] a) S. Gonzalez-Carrero, R. E. Galian, J. Perez-Prieto, *J. Mater. Chem. A* **2015**, *3*, 9187 – 9193; b) H. Huang, A. S. Susha, S. V. Kershaw, T. F. Hung, A. L. Rogach, *Adv. Sci.* **2015**, *2*, 1500194; c) F. Zhang, H. Zhong, C. Chen, X.-g. Wu, X. Hu, H. Huang, J. Han, B. Zou, Y. Dong, *ACS Nano* **2015**, *9*, 4533 – 4542; d) B. Luo, Y.-C. Pu, S. A. Lindley, Y. Yang, L. Lu, Y. Li, X. Li, J. Z. Zhang, *Angew. Chem. Int. Ed.* **2016**, *55*, 8864 – 8868; *Angew. Chem.* **2016**, *128*, 9010 – 9014.

[4] a) A. Swarnkar, R. Chulliyil, V. K. Ravi, M. Irfanullah, A. Chowdhury, A. Nag, *Angew. Chem. Int. Ed.* **2015**, *54*, 15424 – 15428; *Angew. Chem.* **2015**, *127*, 15644 – 15648; b) Y. Bekenstein, B. A. Koscher, S. W. Eaton, P. D. Yang, A. P. Alivisatos, *J. Am. Chem. Soc.* **2015**, *137*, 16008 – 16011; c) X. Li, Y. Wu, S. Zhang, B. Cai, Y. Gu, J. Song, H. Zeng, *Adv. Funct. Mater.* **2016**, *26*, 2435 – 2445; d) J. Song, J. Li, X. Li, L. Xu, Y. Dong, H. Zeng, *Adv. Mater.* **2015**, *27*, 7162 – 7167; e) Y. Wang, X. Li, J. Song, L. Xiao, H. Zeng, H. Sun, *Adv. Mater.* **2015**, *27*, 7101 – 7108.

[5] a) J. A. Sichert, Y. Tong, N. Mutz, M. Vollmer, S. Fischer, K. Z. Milowska, R. García Cortadella, B. Nickel, C. Cardenas-Daw, J. K. Stolarczyk, A. S. Urban, J. Feldmann, *Nano Lett.* **2015**, *15*, 6521 – 6527; b) P. Tyagi, S. M. Arveson, W. A. Tisdale, *J. Phys. Chem. Lett.* **2015**, *6*, 1911 – 1916; c) D. Di, K. P. Musselman, G. Li, A. Sadhanala, Y. Ievskaya, Q. Song, Z.-K. Tan, M. L. Lai, J. L. MacManus-Driscoll, N. C. Greenham, R. H. Friend, *J. Phys. Chem. Lett.* **2015**, *6*, 446 – 450; d) F. Zhu, L. Men, Y. Guo, Q. Zhu, U. Bhattacharjee, P. M. Goodwin, J. W. Petrich, E. A. Smith, J. Vela, *ACS Nano* **2015**, *9*, 2948 – 2959; e) F. Palazon, F. Di Stasio, Q. A. Akkerman, R. Krahne, M. Prato, L. Manna, *Chem. Mater.* **2016**, *28*, 2902 – 2906; f) S. Pathak, N. Sakai, F. Wisnivesky Rocca Rivarola, S. D. Stranks, J. Liu, G. E. Eperon, C. Ducati, K. Wojciechowski, J. T. Griffiths, A. A. Haghighirad, A. Pellaroque, R. H. Friend, H. J. Snaith, *Chem. Mater.* **2015**, *27*, 8066 – 8075; g) V. A. Hintermayr, A. F. Richter, F. Ehrat, M. Döblinger, W. Vanderlinden, J. A. Sichert, Y. Tong, L. Polavarapu, J. Feldmann, A. S. Urban, *Adv. Mater.* **2016**, DOI: 10.1002/adma.201602897; h) S. Yakunin, L. Protesescu, F. Krieg, M. I. Bodnarchuk, G. Nedelcu, M. Humer, G. De Luca, M. Fiebig, W. Heiss, M. V. Kovalenko, *Nat. Commun.* **2015**, *6*, 8056.

[6] L. Protesescu, S. Yakunin, M. I. Bodnarchuk, F. Krieg, R. Caputo, C. H. Hendon, R. X. Yang, A. Walsh, M. V. Kovalenko, *Nano Lett.* **2015**, *15*, 3692 – 3696.

[7] Q. A. Akkerman, S. G. Motti, A. R. Srimath Kandada, E. Mosconi, V. D'Innocenzo, G. Bertoni, S. Marras, B. A. Kamino, L. Miranda, F. De Angelis, A. Petrozza, M. Prato, L. Manna, *J. Am. Chem. Soc.* **2016**, *138*, 1010.

[8] S. Sun, D. Yuan, Y. Xu, A. Wang, Z. Deng, *ACS Nano* **2016**, *10*, 3648 – 3657.

[9] E. T. Hoke, D. J. Slotcavage, E. R. Dohner, A. R. Bowring, H. I. Karunadasa, M. D. McGehee, *Chem. Sci.* **2015**, *6*, 613 – 617.

[10] a) S. Gonzalez-Carrero, G. M. Espallargas, R. E. Galian, J. Perez-Prieto, *J. Mater. Chem. A* **2015**, *3*, 14039 – 14045; b) Z. Yuan, Y. Shu, Y. Tian, Y. Xin, B. Ma, *Chem. Commun.* **2015**, *51*, 16385 – 16388.

[11] J. Feldmann, G. Peter, E. O. Gobel, P. Dawson, K. Moore, C. Foxon, R. J. Elliott, *Phys. Rev. Lett.* **1987**, *59*, 2337 – 2340.

[12] J. Pan, S. P. Sarmah, B. Murali, I. Dursun, W. Peng, M. R. Parida, J. Liu, L. Sinatra, N. Alyami, C. Zhao, E. Alarousu, T. K. Ng, B. S. Ooi, O. M. Bakr, O. F. Mohammed, *J. Phys. Chem. Lett.* **2015**, *6*, 5027 – 5033.

[13] M. A. Green, A. Ho-Baillie, H. J. Snaith, *Nat. Photonics* **2014**, *8*, 506 – 514.

Received: June 20, 2016
Revised: August 11, 2016
Published online: ■■ ■■, ■■■■

 © 2016 Wiley-VCH Verlag GmbH & Co. KGaA, Weinheim

These are not the final page numbers!

Communications

Perovskite Nanostructures

Y. Tong, E. Bladt, M. F. Aygüler, A. Manzi, K. Z. Milowska, V. A. Hintermayr, P. Docampo, S. Bals,* A. S. Urban,* L. Polavarapu,* J. Feldmann ——— ▮▮▮▮–▮▮▮▮

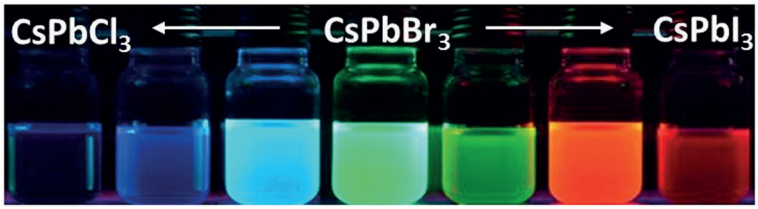

Highly Luminescent Cesium Lead Halide Perovskite Nanocrystals with Tunable Composition and Thickness by Ultrasonication

Under ultrasonication: Perovskite nanocrystals and nanoplatelets with controlled halide composition and thickness were prepared by direct ultrasonication of the corresponding precursor solutions in the presence of organic capping molecules. The optical properties of the as-prepared $CsPbX_3$ NCs can be tuned across the entire visible range by changing either the composition or thickness.

© 2016 Wiley-VCH Verlag GmbH & Co. KGaA, Weinheim